

Article

Effects of Long-Term Aging on Structure Evolution and Stress Rupture Property of DD6 Single-Crystal Superalloy

Weiwei Liu *, Shizhong Liu, Ying Li and Jiarong Li

Science and Technology on Advanced High Temperature Structural Materials Laboratory, AECC Beijing Institute of Aeronautical Materials, Beijing 100095, China

* Correspondence: liuww_80@sina.com

Abstract: For China's second-generation aero-engine blade DD6 single-crystal high-temperature alloy, the standard solution-treated test rods were subjected to long-term aging experiments (1290 °C, 1 h + 1300 °C, 2 h + 1315 °C, 4 h air cooling + 1120 °C, 4 h air cooling + 870 °C, 32 h air cooling) at 980 °C for 1000 h, 5000 h, and 7500 h, and the effects of different long-term aging times on the organization evolution, phase precipitation morphology, high-temperature mechanical properties, and endurance performance of the alloy were studied. The results show that with the increase of aging time, the γ' phase coarsens, joins along the $\langle 100 \rangle$ and $\langle 010 \rangle$ directions, and merges to form irregularly shaped directional growth and rafting. The endurance life shows a decreasing trend; at 980 °C/243 MPa, 980 °C/270 MPa, 980 °C/309 MPa for the alloys after 5000 h aging, the enduring life decreased by 47.97%, 70.98%, and 76.75%, and 81.25%, 73.18%, and 87.00% after 7500 h aging, respectively. The tensile strength of the alloy at 760 °C first decreases and then increases, with a minimum value at 5000 h; there is a gradual increase in elongation; there is a gradual decrease in tensile strength at 980 °C; and there is first an increase and then decrease in elongation, with a maximum value at 1000 h. This is due to the diffusion phenomenon of the elements in the alloy after 5000 h aging, the emergence of W-rich, Re-, Mo-, and Ni-poor phenomena, and the transformation of the μ -phase from needle-like to rod-like and block-like.

Keywords: DD6 single-crystal superalloy; long-term aging; stress rupture property; tensile properties; structure evolution



Citation: Liu, W.; Liu, S.; Li, Y.; Li, J. Effects of Long-Term Aging on Structure Evolution and Stress Rupture Property of DD6 Single-Crystal Superalloy. *Metals* **2023**, *13*, 1063. <https://doi.org/10.3390/met13061063>

Academic Editor: Alberto Moreira Jorge Junior

Received: 13 March 2023
Revised: 25 April 2023
Accepted: 8 May 2023
Published: 1 June 2023



Copyright: © 2023 by the authors. Licensee MDPI, Basel, Switzerland. This article is an open access article distributed under the terms and conditions of the Creative Commons Attribution (CC BY) license (<https://creativecommons.org/licenses/by/4.0/>).

1. Introduction

The Ni-based single-crystal superalloy features excellent high-temperature mechanical properties, a high anti-fatigue ability, and creeping resistance, and is widely used in the turbine blades of aircraft engines and gas turbines as well as other thermal end parts [1–8]. DD6 single-crystal alloy is the second-generation low-cost Ni-based single-crystal superalloy developed by China. In addition to low Re content, DD6 has tensile properties and a creep rupture resistance that is comparable to those of the second-generation single-crystal superalloys outside of China [9]. Thus, DD6 has an evident cost advantage and is widely studied by researchers from China and other countries.

The main strengthening phase in the DD6 alloy is the γ' phase, which is distributed in the cubic state in the matrix after thermal treatment. The volume fraction, size, distribution state, cubic metric of the γ' phase, and the degree of lattice misfit with the γ phase in the matrix all affect the mechanical properties of the alloy [10–13]. The method of γ' phase formation has been reported to have a significant effect on various properties of the alloy [14–19]. When the γ' phase is uniformly and regularly distributed with a volume fraction of 65–70% and a size of 0.45–0.5 μm , its comprehensive mechanical performance is the optimal performance. During the design of this alloy, however, to improve its high-temperature mechanical performance, refractory elements in a large atom radius (W, Mo, Re) were added, and an excellent solid-solution strengthening effect was achieved through thermal treatment. However, a large quantity of refractory elements at

high temperatures increased the tendency of the precipitate topological dense phase (TCP). In the meantime, Re or Cr binds with C to form carbide precipitates, which increase the tendency of brittle rupturing in the alloy. As for the evaluation of service performance, since the alloy shall be thermally exposed for a long time at a high temperature, the cubic metric of the γ' phase gradually decreases or is structurally rafted, and the γ' phase redissolves and degrades, which significantly weakens the mechanical properties of the alloy. Thus, research on the structural stability and high-temperature stress rupture property of the DD6 under actual service conditions is very important. Zhao Y. et al. studied the effects of thermal isostatic pressing on the microstructure defects, and of the stress rupture property on the second-generation solid-solution single-crystal superalloy, and clarified the mechanism of how thermal isostatic pressing improved the structural state and the stress rupture property of the Ni-based alloy under different initial structural states [20]. Lv et al. studied the microstructure and creep properties of two low-cost single crystal superalloys under different creep conditions and found that the high-Re-alloy γ' phase microstructure had better stability and a smaller deformation degree at high temperatures [21]. However, the γ' phase started to be rafted at 980 °C/250 MPa and was severely rafted at 1100 °C/140 Mpa. Moreover, the fourth-generation single-crystal superalloy DD15 under independent development was studied in terms of the stress rupture performance at three orientations ([001], [011], [111]), and the stress rupture property and rupture mechanism of the alloy at different orientations at 980 °C/300 Mpa were explored. Zhao et al. [22] studied the microstructure and properties of a low-cost nickel-based single-crystal superalloy and found that the cubic degree and size of the γ' phase have a great influence on the alloy's properties, and that a high cubic degree and an appropriate volume fraction can improve the alloy's properties. The volume fraction and size of micropores both significantly decreased after the thermal isostatic pressing, and the stress rupture life was significantly prolonged under both 850 °C/650 MPa and 1100 °C/170 MPa. To meet the service performance requirements of the second-generation single-crystal superalloy, Liu Lin et al. [23] studied the microstructure evolution, mechanical properties, and durability of an alloy containing 2% Re after long-term aging at 900 °C for 2000 h. Yang et al. [24] studied the microstructure and mechanical properties of a second-generation alloy after long-term aging at 1000 °C to 1100 °C and discussed the correlation between microstructure and mechanical properties. The changing rules of microstructures and mechanical properties after aging and the effects of long-term aging on stress rupture properties were clarified. However, along with the gradual improvement in aircraft engine design indices, the requirement for the service life of key parts is significantly raised. To ensure the long-term and stable service status of blades, the effects of structural stability on mechanical properties during the long-term serving process shall be simulated. Among the existing studies, the longest aging time in the simulation of actual serving conditions by using long-term aging methods is 2000 h. However, there is no report about the microstructure evolution and mechanical property changes in the DD6 single-crystal superalloy when the aging time is longer than 2000 h.

In this study, targeting the second-generation single-crystal superalloy DD6 developed independently by China, long-term aging after 1000 h, 5000 h, and 7500 h was conducted under load-free conditions in air at 980 °C. The aged alloy bars were sent to be high-temperature tension tested and stress rupture tested. Then, the rules of microstructure evolution and the stress rupture characteristics of this alloy during long-term aging were tested via microstructure characterization. Thereby, the mechanism showed how long-term aging affected the alloy performance. The findings will offer a theoretical basis and data support for the future application of DD6 single-crystal superalloy into aircraft engines.

2. Experimental Section

DD6 bars in the [001] orientation were prepared in a vacuum induction directional solidification furnace using spiral crystal selection. The chemical composition of the

parent alloy (purity > 99.9%) is shown in Table 1. The crystallization orientation of the single-crystal bars was tested using the Laue X-ray method. The deviation of the [001] crystallization orientation from the principal stress axis of the specimen was less than 15°. The DD6 alloy bars were thermally treated under vacuum in a standard method. The thermal treatment conditions were 1290 °C, 1 h + 1300 °C, 2 h + 1315 °C, 4 h air cooling + 1120 °C, 4 h air cooling + 870 °C, and 32 h air cooling (standard thermal treatment).

Table 1. Chemical composition of DD6 single-crystal superalloy (weight, wt%).

Cr	Co	Mo	W	Re	Ta	Nb	Al	Hf	C
4.3	9	2	8	2	7.5	0.5	5.6	0.1	0.006

The thermally treated bars were aged for the long term (1000, 5000, 7500 h) in the air at 980 °C and without load. The aged specimens were tested in terms of high-temperature tensile ability and stress rupture property (standard of execution: GB/T 38822-2020). The conditions were 980 °C/309 MPa, 980 °C/270 MPa, and 980 °C/243 MPa, and the temperatures in the high-temperature tensile tests were 980 or 760 °C. All experiments were not stopped until the specimens ruptured. The shape and size of the stress rupture specimens are shown in Figure 1. The 0.2 mm sample was cut close to the creep fracture and perpendicular to the stress direction. After grinding with sandpaper, the sample was electrolytically polished with 20 mL H₂SO₄ + 80 mL CH₃OH electrolyte (25~30 V, 15~20 s). Then, it was etched in 8 g CrO₃ + 85 mL H₃PO₄ + 5 mL H₂SO₄ electrolyte (5 V, 3~5 s). The microstructure and fracture morphology of the tensile specimens were observed under an S3400N scanning electron microscope (Hitachi, Toyohashi, Japan). Near the creep fracture, a 0.2 mm slice was cut perpendicular to the stress direction and thinned to less than 40 µm with sandpaper. Then, the samples were prepared by the twin-jet electropolishing method with an electrolytic double spray solution of 10% HClO₄ + 90% CH₃COOH (50~70 V, 30~50 mA, −25 °C). The morphology, size, and type of precipitated phases were characterized under a JEM-2100 transmission electron microscope (Nippon Electron Corporation, Akishima, Japan). For the calculation of the γ phase and γ' phase sizes in Figure 2, the linear intercept method is used, which means that the field of view in the figure is selected to make a straight line, and the average intercept between the phases is calculated by observing the number of nodes through the formula [25], where d is the average grain size of the alloy and L is the linear intercept grain size.

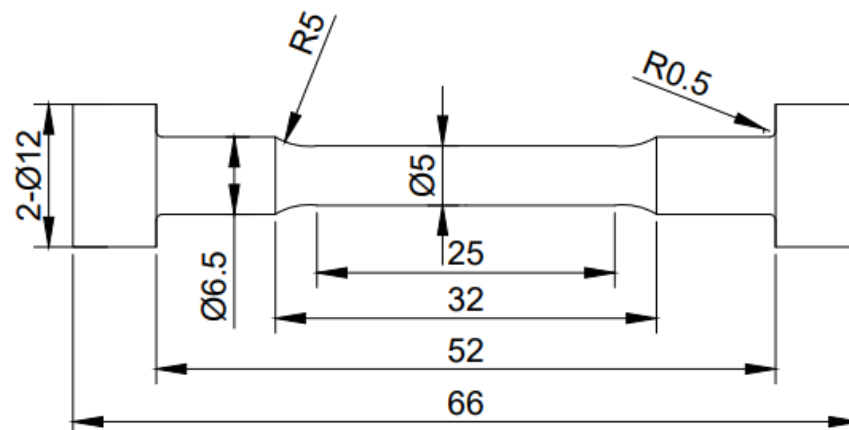


Figure 1. Diagram of a stress rupture sample (units in mm).

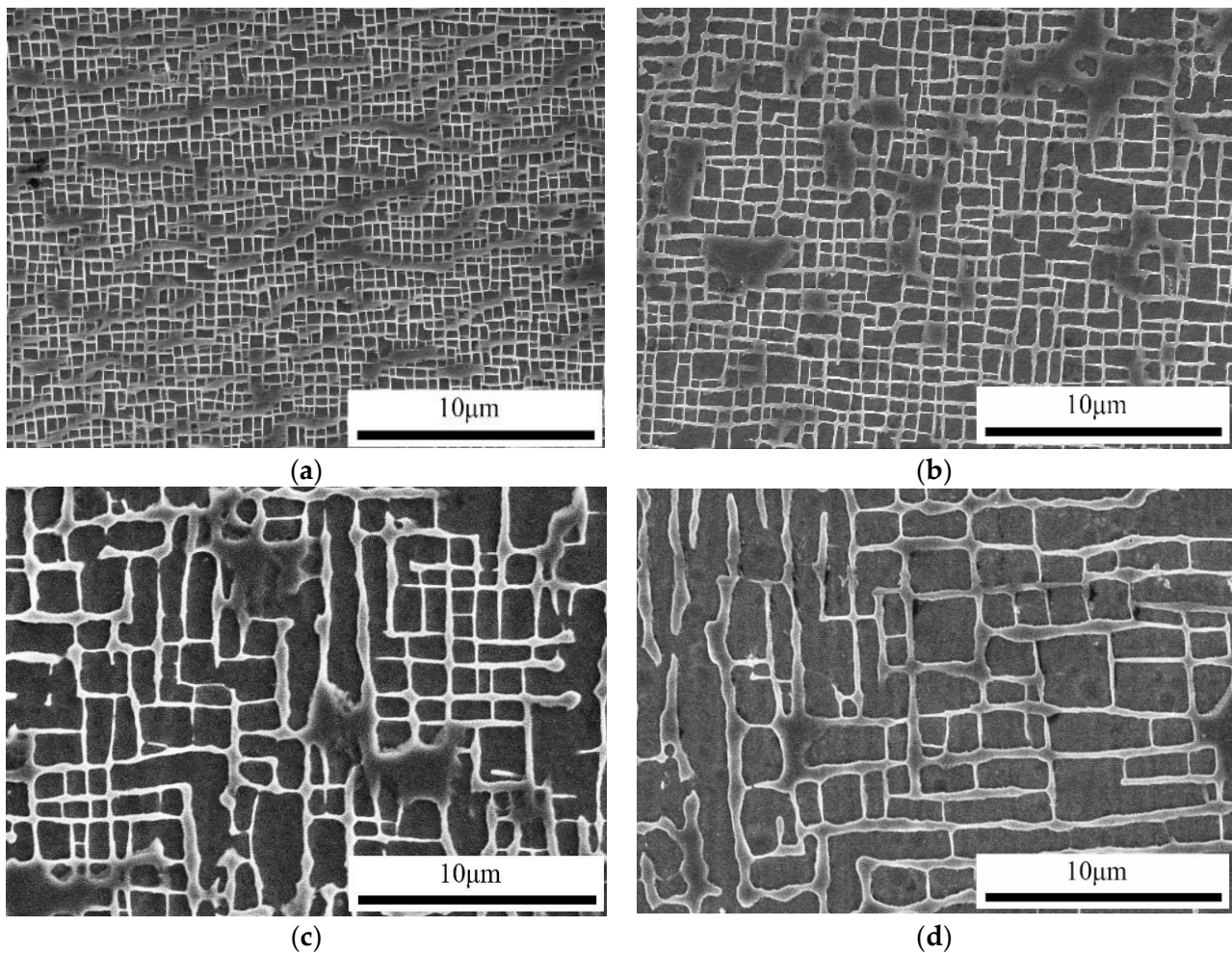


Figure 2. Microstructure morphology of the alloy after long-term aging at 980 °C for different times: (a) 0 h; (b) 1000 h; (c) 5000 h; (d) 7500 h.

3. Results and Analysis

3.1. Effects of Long-Term Aging on Structures of DD6 Alloy

Figure 2 shows the microstructure of DD6 alloy after long-term aging for a certain time obtained by SEM. After the thermal treatment (1290 °C, 1 h 1300 °C, 2 h + 1315 °C, 4 h air cooling + 1120 °C, 4 h air cooling + 870 °C, 32 h air cooling), the γ' phase was cubic and uniformly distributed (Figure 2a). The average size and volume fraction were calculated using the intercept method to be 0.48 μm and 63%, respectively. When the above alloy was aged in air for long time (1000, 5000, 7500 h) at 980 °C, the γ' phase grew up with the prolonging of aging time. Meanwhile, the channel width of the γ matrix was enlarged, the γ' phase was marginally passivated, and the cubic metric gradually decreased. Figure 3a shows the relationship curve between the γ' phase and the long-term aging time. Clearly, the sizes of the γ' phase under the above aging time periods were 0.48, 0.81, 1.16, and 1.43 μm , respectively. When the aging time was longer than 5000 h, the size of the γ' phase exceeded 1 μm . Size computation of the γ' phase showed the local γ' phase was coarsened, connected, and combined. When the aging time was shorter than 1000 h, the γ' phase was coarsened, but it reserved the cubic shape. Compared with the structures without aging, the overall morphology did not change greatly (Figure 2a) and no TCP was separated out, which are consistent with other studies [15,24]. When the aging time was up to 5000 h, the size of the γ' phase was significantly enlarged, the matrix channels were broadened, and the cubic degree of the γ' phase decreased. The γ' phase connected and combined along the $\langle 100 \rangle$ and $\langle 010 \rangle$ directions to form irregular strips and an L shape. Moreover, evident

rafting occurred and, finally, the γ' phase directionally grew up, forming rafting structures (Figure 2c). When the aging time was 7500 h, the structure morphology was similar to that after 5000 h of treatment, and the structure rafting was more significant (Figure 2d). These results indicate the size of the γ' phase changed and its shape varied along with the prolonging of aging time. Therefore, the mechanism of γ' phase transformation in DD6 alloy after long-term aging shall be analyzed.

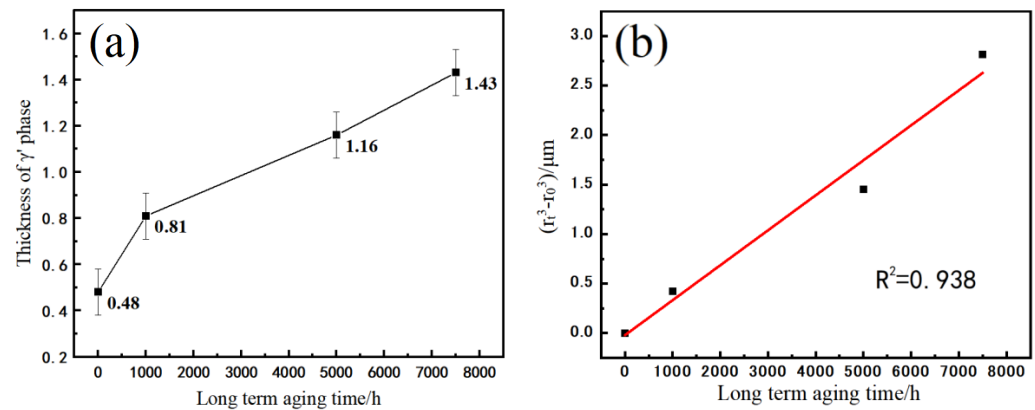


Figure 3. Relationship between γ' phase size and long-term aging time: (a) measured value; (b) relationship between $r_t^3 - r_0^3$ and aging time.

In the Ni-based single-crystal superalloy, the element compositions are different between the matrix γ phase and the secondary γ' phase. Thus, element redistribution will occur during long-term aging. Specifically, the γ' phase-forming elements (Al, Ta, Hf, Nb) diffuse to the matrix, increasing the size of the γ' phase, but Re, W, and Mo in the matrix diffuse to the γ' phase, enlarging the channel width of the matrix. Moreover, the γ' phase growing process satisfies the Ostwald model. Namely, the large-size γ' phase grows up, but the small-size γ' phase dissolves. This is because during the long-term aging, the solute concentration around small grains is larger than that around large grains, which makes the solute atoms around small grains diffuse to the vicinity of large grains. The diffusion destroys the balance of solute concentrations around grains, resulting in the dissolution of small grains and the growth of large grains, which is consistent with some other studies [26,27]. It is generally accepted that in nickel-based single-crystal superalloys, the coarsening of the γ' phase proceeds according to Ostwald ripening and conforms to the Lifshitz–Slyozov–Wagner (LSW) law, as shown in the following Equation [27]:

$$r_t^3 - r_0^3 = Kt, \quad (1)$$

where r_0 and r_t are the dimensions of the γ' phase after initial time and aging t time, respectively, and k is the growth rate of the γ' phase, which can be expressed as follows:

$$k = \frac{8}{9} \cdot \frac{D_s \cdot \sigma_{\gamma'}^{\frac{\gamma}{\gamma'}} \cdot V_M^2}{R \cdot T}, \quad (2)$$

where D_s is the diffusion coefficient of the solute element in the matrix, $\sigma_{\gamma'}^{\frac{\gamma}{\gamma'}}$, and γ is the interfacial energy of the γ' phase, c_0 is the equilibrium concentration of the solute element in the matrix, V_M^2 is the molar volume of the γ' phase, R is the gas constant, and T is the thermodynamic temperature. Therefore, the size (r) of the γ' phase is in accordance with the $r_3 \propto k \cdot t$ law. The temperature is constant at long-term high-temperature aging, D , $\sigma_{\gamma'}^{\frac{\gamma}{\gamma'}}$, and c_0 ; V_M^2 does not change significantly, so k can be approximated as a constant. Based on the data in Figure 3a, the relation curve between the average radius of the γ' phase and the long-term aging time can be clarified through linear fitting (Figure 3b). Clearly, on the fitted curve, an approximately linear relationship between $r_t^3 - r_0^3$ and aging time t was

found, with the fitting precision, R , of 0.972 indicating that this fitting result obeys the LSW model. However, compared with the 1000 h of aging, the data points at the aging time longer than 5000 h slightly deviate, which is because the γ' phase was not only coarsened and grew up with the aging; it also changed in shape (Figure 3b–d). In all, the coarsening, growth, connection, and combination of the γ' phase during long-term aging of the DD6 alloy are essentially closely correlated with the diffusion of alloy elements.

3.2. Effects of Long-Term Aging on Tensile Properties of DD6 Alloy

The tensile properties of the thermally treated DD6 alloy and long-term aged DD6 alloy at 760, 980 °C, are shown in Table 2. Clearly, the tensile strength and yield strength at 980 °C are both lower than those at 760 °C. Moreover, the tensile strength and yield strength after long-term aging are both lower than and the elongation at break, and the section contraction rate is larger than that after thermal treatment regardless of the temperature. Figure 4 shows the tensile property curves of this alloy at different aging temperatures. As the aging time was prolonged at 760 °C, the elongation at break of the alloy gradually increased, but the tensile strength first declined and then rose, with a minimum appearing after 5000 h. When the aging time was 7500 h, the tensile strength of the alloy increased by 27 MPa and the elongation rate rose by 4%, which showed better comprehensive mechanical performance compared with the aging time of 5000 h. As the aging time was prolonged at 980 °C, the tensile strength was gradually weakened, but the elongation at break did not change greatly and varied within 27–29.7%. The variation in the high-temperature tensile properties of this alloy with the temperature was closely related to dislocation motion. At the high temperature (980 °C), the γ' phase was softened. Because of low strength, the inhibition of the γ' phase against dislocation motion was weakened after the softening, as abundant dislocations cut into the γ' phase, leading to a significant decrease in strength. In the meantime, the high temperature allowed a large number of slip systems in the alloy to be activated, so its deformability was increased along with larger plasticity and elongation rate.

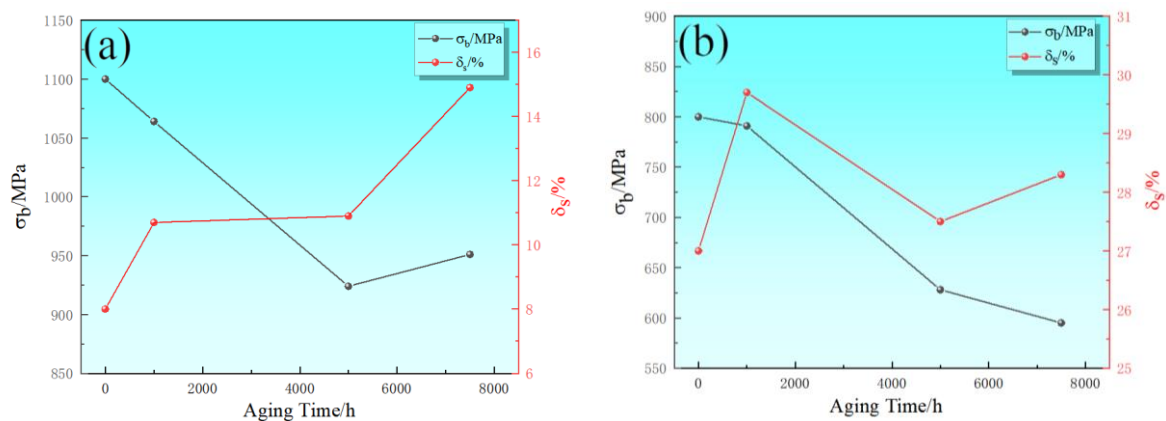


Figure 4. High-temperature tensile properties of DD6 alloy under thermal treatment or under long-term aging at (a) 760 °C; (b) 980 °C.

Table 2. High-temperature tensile properties of DD6 alloy under thermal treatment or under long-term aging at 980 °C.

Test Temperature/°C	Aging Time/h	UTS/ σ_b /MPa	YS/ $\sigma_{0.2}$ /MPa	A_5/δ_5 /%	ψ /%
760	0	1100	935	8	12
	1000	1064	904	10.7	15.1
	5000	924	826	10.9	21.9
	7500	951	820	14.9	28.3

Table 2. Cont.

Test Temperature/°C	Aging Time/h	UTS/ σ_b /MPa	YS/ $\sigma_{0.2}$ /MPa	A_5/δ_5 /%	ψ /%
980	0	800	680	27	34
	1000	791	686	29.7	31.5
	5000	628	581	27.5	28.3
	7500	595	525	28.3	29.2

Then, the product of tensile strength and elongation ($\sigma_b \times \delta_s$ /GPa%) was introduced to better reflect the strong plastic matching rule of the alloy at 760 or 980 °C. Figure 5 shows the schematic diagram of the strong plasticity matching rule. The product of tensile strength and elongation of the alloy with the aging time at 980 °C was computed to be 0.216, 0.235, 0.173, and 0.168 GPa%, respectively, indicating the product of tensile strength and elongation after 1000 h of aging was larger than that after thermal treatment. The product of tensile strength and elongation was reduced with the prolonging of aging time, but it did not change substantially beyond the aging time of 5000 h. The product of tensile strength and elongation with the aging time at 760 °C was 0.088, 0.114, 0.101, and 0.142 GPa%, respectively, indicating the product of tensile strength and elongation was the smallest when no aging was adopted. At this moment, the alloy strength was high, but the plasticity was low, and the alloy strength did not decrease largely after long-term aging, although the plasticity was significantly increased. In all, at high temperature, the long-term aging largely affected the mechanical properties of the DD6 alloy, and this effect was especially significant when the aging time exceeded 5000 h.

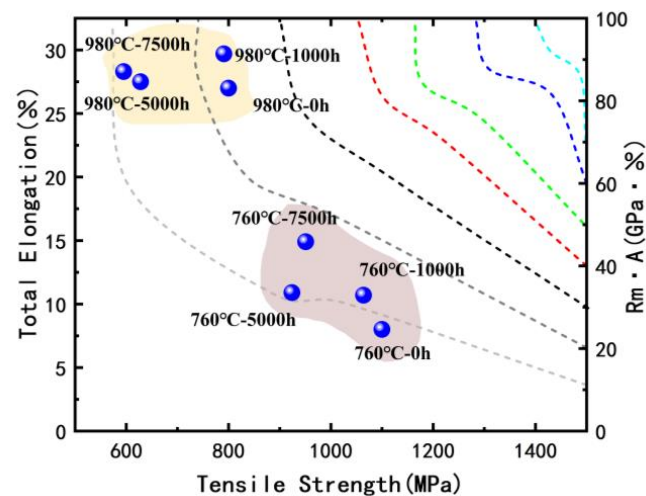


Figure 5. The schematic representation of the strong plastic matching rule.

3.3. Effects of Long-Term Aging on Stress Rupture Property of DD6 Alloy

Figure 6 shows the tensile curves at different aging temperatures at 980 °C. The results of stress rupture property in the DD6 after standard thermal treatment or long-term aging are listed in Table 3. Comparison, under the same aging time, showed that the stress rupture life of the thermally treated specimens or the long-term aged specimens was shortened with the increase of applied stress. When the stress rupture test conditions were the same, the stress rupture life was shortened with the prolonging of aging time. After 1000 h of aging, the stress rupture life was shortened by 24.27%, 31.47%, and 27.58% with the increase of applied stress (243, 270, and 309 MPa, respectively) compared with the standard thermal treatment. After 5000 h of aging, the stress rupture life decreased by 47.97%, 70.98%, and 76.75%, respectively, and the stress rupture life was shortened by 81.25%, 73.18%, and 87.00%, respectively, after 7500 h of aging. These results indicate the service

life was significantly shortened when the aging time exceeded 5000 h. This was because after the aging time was beyond 5000 h, the size of the γ' phase significantly enlarged, the matrix channels were broadened, and the cubic degree of the γ' phase decreased. Moreover, irregular strips and an L shape were formed after connection and combination, and finally, raft-like structures were formed after directional growth, which weakened the resistance of the γ' phase against dislocation and thereby largely shortened the stress rupture life.

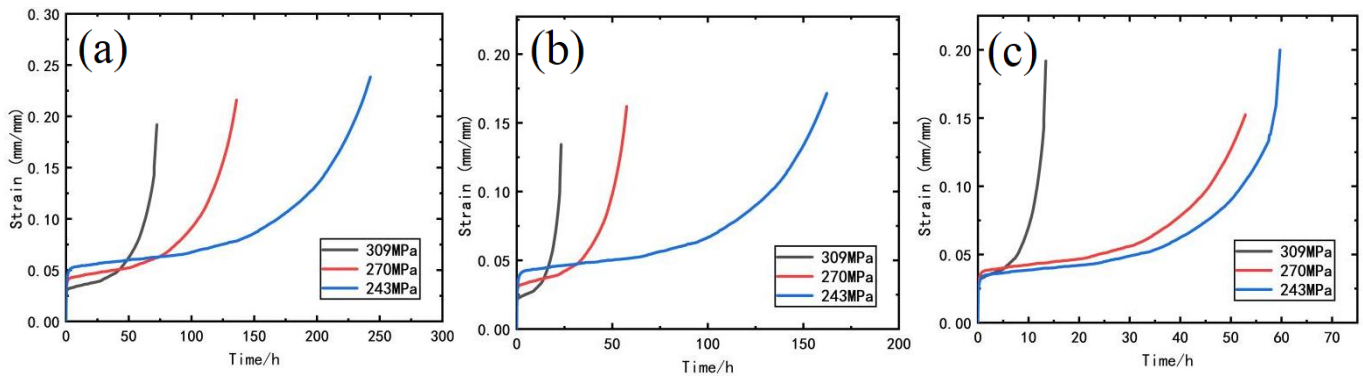


Figure 6. Tensile curves at different aging temperatures at 980 °C: (a) 1000 h; (b) 5000 h; (c) 7500 h.

Table 3. Stress rupture property of alloy after thermal treatment or after long-term aging at 980 °C.

Aging Time/h	Stress/MPa	Stress Rupture Life of Heat Treated Alloy/h	After Long-Term Aging for Stress Rupture Life of Alloy	Proportion of Corresponding Life
1000	309	100	72.42	72.42%
	270	197	135.00	68.53%
	243	320	242.33	75.73%
5000	309	100	23.25	23.25%
	270	197	57.16	29.02%
	243	320	166.50	52.03%
7500	309	100	13.00	13.00%
	270	197	52.84	26.82%
	243	320	60.00	18.75%

Analysis of the stress rupture property data in Table 3 showed the applied stress and aging time jointly affected the stress rupture life of the alloy. After 1000 h of aging, the stress rupture life of the DD6 alloy was not largely affected by the applied stress. Compared with the standard thermal treatment, the decreasing rate in the stress rupture life of the alloy maximized to 31.47% at the stress of 270 MPa. After 5000 h of aging, the stress rupture life of the alloy was shortened with the increase of the applied stress, and the decreasing rate in the stress rupture life maximized at the lowest stress (270 MPa). After 7500 h of aging, the stress rupture life of the alloy was greatly shortened and maximized at the lowest stress (243 MPa). The above analysis indicates that though the stress rupture life of this alloy is shortened with the increase of applied stress, the shortening rate of stress rupture life increases and is largely affected by the aging time. When the aging time is 5000 or 7500 h, the shortening rate of durable lifetime maximizes at low stress. This is due to the fact that no precipitation phase was found after aging at 980 °C for 1000 h. When the aging time was 5000 h and 7500 h, needle-like, rod-like, and polygonal block-like μ -phase appeared, characterized by rich W, Re, and Mo and poor Ni. Meanwhile, as the W/Mo value decreases, the μ phase has a multi-variable transition trend from needle-like to rod-like and block-like. It is shown that γ' phase rafting and μ phase precipitation and shape change have an important effect on the alloy persistence properties. This implies that the stress rupture life of the DD6 alloy is significantly affected by the interaction of aging time and applied stress.

4. Discussion

When the Ni-based alloy was aged for a long time, the morphology, size, and volume fraction of its γ' phase and the separation of TCP all largely affected the mechanical properties and stress rupture property of the alloy. When the size of the γ' phase was 0.48–0.81 μm , the volume fraction was 63–69%, and the cubic degree was well distributed, dislocation motion could be effectively inhibited, so the alloy had excellent mechanical performance. When the aging time was 5000 or 7500 h, the γ' phase grew up, and under the regulation of interface energy, the shape of the γ' phase changed, increasing the lattice misfit degree of γ/γ' phases. During the high-temperature stress rupture experiments, the strength degradation in the γ' phase led to a decrease in stress rupture strength. Meanwhile, the dislocation climbed and shifted under the action of high thermal activation energy. The dislocation motion has to overcome Orowan resistance τ . The relationship between τ and the matrix channel width is shown below:

$$\tau = \sqrt{\frac{2}{3}} \frac{\mu b}{h}, \quad (3)$$

where μ is the shear modulus, b is Burgers vector, and h is the matrix channel width. When the aging time was 5000 or 7500 h, the γ matrix channel width was enlarged. Based on the above equation, the increase of h led to a decrease in the Orowan resistance τ ; namely, the inhibition against dislocation motion in matrix channels was weakened. This is the main reason for the decrease in the stress rupture property after long-term aging.

When the aging time was shorter than 1000 h, no TCP was found in the alloy. When the aging time was 5000 or 7500 h, three shapes were separated out in between dendritic crystals, including the needle shape, bar shape, and polygonal blocks (Figure 7). An evident interface was found between any shape of the precipitate phase and the matrix. Then, the micro-district diffraction spots of the precipitate phase were calibrated and analyzed. This phase had a complex triangular crystal structure, with lattice constants $a = 0.4865 \text{ nm}$ and $c = 2.4732 \text{ nm}$. The EPMA results of the needle-shaped precipitate phase are listed in Table 4. Compared with the nominal composition of the DD6 alloy, the precipitate phase was rich in W, Re, and Mo and had a low content of Ni, and the contents of Nb, Cr, and Co were not greatly different from the nominal composition (Table 4). The richness in W, Re, and Mo and the deficiency in Ni are characteristic of the μ phase and M6C [27–30]. Together with the structural analysis of the precipitate phase in Figure 7, the precipitate phase was determined to be the μ phase. The difference in the content ratio of W to Mo (W/Mo) was the major cause for the different shapes in the precipitate phase. Based on Table 4, the W/Mo ratios of the precipitate phase in the different shapes (needle shape, bar shape, and polygonal blocks) were computed to be 2.11, 2.01, and 1.27, respectively (Table 4). These results indicate as the W/Mo ratio decreased, the morphology of the precipitate phase transitioned from the needle shape to the bar shape and polygonal blocks, indicating the precipitate phase tended to be polygons. The precipitation of the μ phase depleted the high-melting-point elements in the matrix, decreasing the solid solution strengthening effect, and the precipitation of the refractory elements intensified the diffusion of other alloy elements in between the γ/γ' phases, weakening the γ' phase and the γ/γ' interface. The precipitate phase transitioned to polygons, so the TCP inhibited dislocation motion in the alloy, and restricted the resistance of γ' -phase-raftered structures against dislocation, thus accelerating the formation and expansion of crack TCP. This was one of the reasons why the stress rupture property of this alloy was significantly weakened after 5000 or 7500 h of aging.

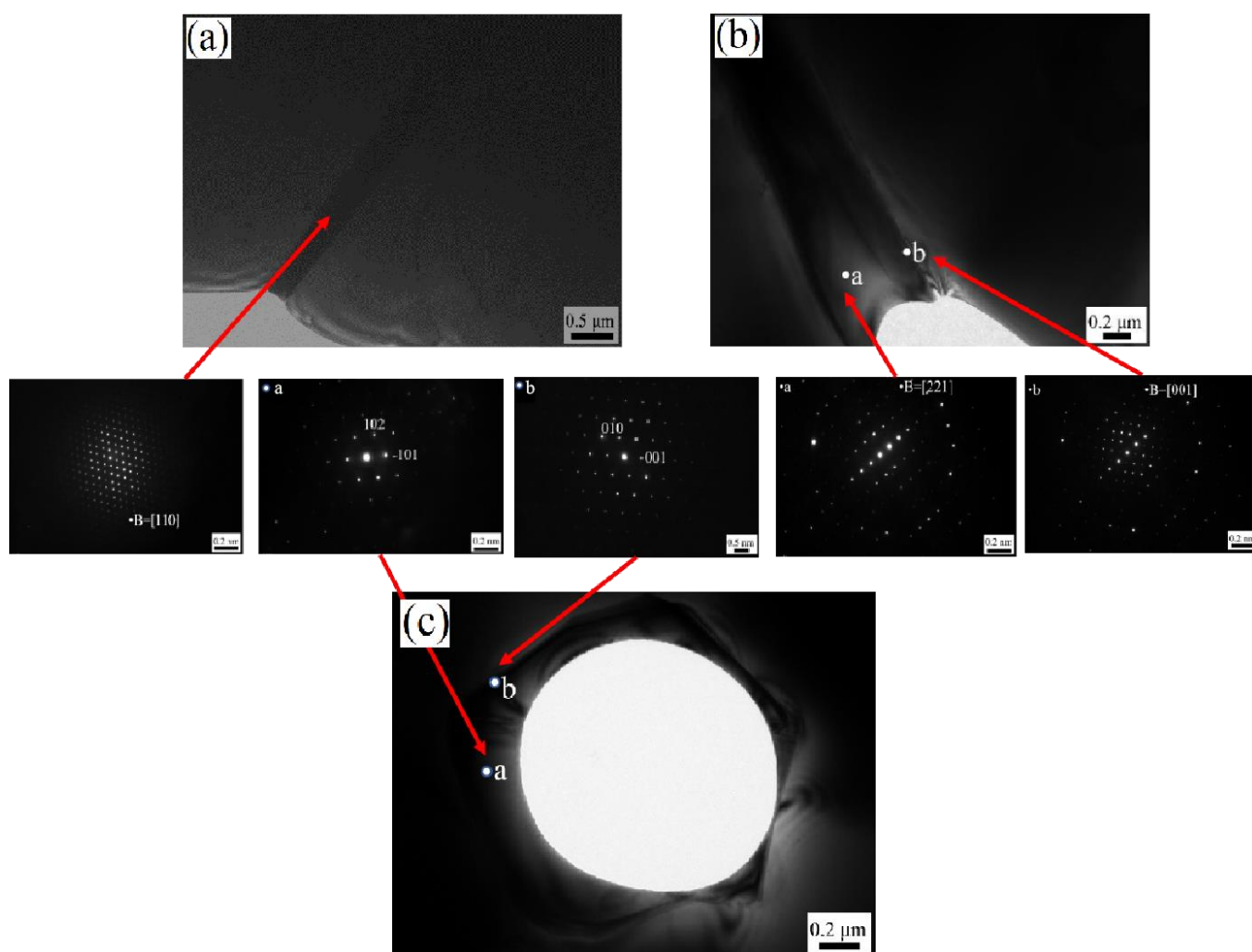


Figure 7. Morphology and diffraction patterns of precipitate phases after 5000 h of aging in the DD6 alloy: (a) needle shape; (b) bar shape (c); polygonal blocks.

Table 4. Element contents in the needle-shaped, bar-shaped, and polygonal block precipitate phases (at%).

Shape	C	Cr	Co	Ni	W	Re	Nb	Mo
Needle shape	23.8	10.4	8.5	17.3	23.5	4.0	1.4	11.1
Bar shape	27.8	9.2	7.7	15.4	22.7	4.4	1.4	11.3
Polygonal blocks	11.3	13.8	20.5	21.4	14.3	0.6	6.8	11.3

5. Conclusions

Through the research of this paper, the influence law of the long-term aging time of second generation nickel-based single crystal high-temperature alloy DD6 on its high temperature mechanical properties and creep persistence performance was obtained and explained from the tissue evolution law of matrix-phase γ , high temperature strengthening-phase γ' , and precipitation-phase μ with extended aging time, and the main conclusions drawn are as follows:

1. D6 alloy after 1000 h, 5000 h, and 7500 h long-term aging treatment: for the alloy at 760 °C, the tensile strength first decreases and then increases with the extension of the aging time, and the minimum value appears at 5000 h; at 980 °C, the tensile strength decreases gradually with the extension of the aging time, and the elongation increases

- first and then decreases, reaching the maximum value at 2000 h. With the extension of the aging time, the lasting life is showing a decreasing trend; when the aging time is 7500 h, the lasting life is significantly reduced;
2. With the extension of aging time, the size of the high-temperature strengthening-phase γ' in the matrix gradually increases, the matrix channel widens, and the cubicization of the γ' phase decreases continuously along the $\langle 100 \rangle$ and $\langle 010 \rangle$ directions, connecting and merging to form irregular shapes (such as long strips, L shapes, etc.), and eventually growing directionally to form raft rows;
 3. After aging at 980 °C for 1000 h, no precipitation phase was found. When the aging time was 5000 h and 7500 h, needle-like, rod-like, and polygonal block-like μ phase appeared, characterized by rich W, Re, and Mo and poor Ni. Meanwhile, as the W/Mo value decreases, the μ phase demonstrates a multi-variable transition trend from needle-like to rod-like and block-like.

Author Contributions: Conceptualization, W.L. and S.L.; methodology, W.L.; software, Y.L.; validation, W.L., S.L. and J.L.; formal analysis, W.L.; investigation, S.L.; resources, Y.L.; data curation, W.L.; writing—original draft preparation, W.L.; writing—review and editing, W.L.; visualization, S.L.; supervision, Y.L.; project administration, J.L.; funding acquisition, S.L. All authors have read and agreed to the published version of the manuscript.

Funding: This research received no external funding.

Data Availability Statement: No new data were created or analyzed in this study. Data sharing is not applicable to this article.

Conflicts of Interest: The authors declare no conflict of interest.

References

1. Moverare, J.J.; Johansson, S.; Reed, R.C. Deformation and damage mechanisms during thermal-mechanical fatigue of a single-crystal superalloy. *Acta Mater.* **2009**, *57*, 2266–2276. [[CrossRef](#)]
2. Graverend, J.B.; Cormier, J.; Gallerneau, F.; Villechaise, P.; Kruch, S.; Mendez, J. A microstructure-sensitive constitutive modeling of the inelastic behavior of single crystal nickel-based superalloys at very high temperature. *Int. J. Plast.* **2014**, *59*, 55–83. [[CrossRef](#)]
3. Khomutov, M.G.; Churyumov, A.Y.; Pozdnyakov, A.V.; Voitenko, A.G.; Cheresheva, A.A. Simulation of the kinetics of dynamic recrystallization of alloy KhN₅₅MBYu-VD during hot deformation. *Met. Sci. Heat. Treat.* **2019**, *60*, 606–610. [[CrossRef](#)]
4. Arakere, N.K.; Orozco, E. Analysis of low cycle fatigue properties of single crystal nickel-base turbine blade superalloys. *High Temp. Mater. Process.* **2001**, *20*, 403–420. [[CrossRef](#)]
5. Lizzi, F.; Pradeep, K.; Stanojevic, A.; Sommadossi, S.; Poletti, M.C. Hot Deformation Behavior of a Ni-Based Superalloy with Suppressed Precipitation. *Metals* **2021**, *11*, 605. [[CrossRef](#)]
6. Popova, M.A.; Kuznetsov, V.P.; Lesnikov, V.P.; Popov, N.A.; Konakova, I.P. The structure and mechanical properties of single-crystal nickel alloys with Re and Ru after high-temperature holds. *Mat. Sci. Eng. A Struct.* **2015**, *642*, 304–308. [[CrossRef](#)]
7. Sato, A.; Harada, H.; Yokokawa, T.; Murakumo, T.; Koizumi, Y.; Kobayashi, T.; Imai, H. The effects of ruthenium on the phase stability of fourth generation Ni-base single crystal superalloys. *Scripta Mater.* **2006**, *54*, 1679–1684. [[CrossRef](#)]
8. Yeh, A.C.; Tin, S. Effects of Ru on the high-temperature phase stability of Ni-base single-crystal superalloys. *Metall. Mater. Trans. A* **2006**, *37*, 2621–2631. [[CrossRef](#)]
9. Xiong, X.; Quan, D.; Dai, P.; Wang, Z.; Zhang, Q.; Yue, Z. Tensile behavior of nickel-base single-crystal superalloy DD6. *Mat. Sci. Eng. A* **2015**, *636*, 608–612. [[CrossRef](#)]
10. Long, H.B.; Wei, H.; Liu, Y.N.; Mao, S.C.; Zhang, J.X.; Xiang, S.S.; Chen, Y.H.; Gui, W.M.; Li, Q.; Zhang, Z.; et al. Effect of lattice misfit on the evolution of the dislocation structure in Ni-based single crystal superalloys during thermal exposure. *Acta Mater.* **2016**, *120*, 95–107. [[CrossRef](#)]
11. Hegde, S.R.; Kearsey, R.M.; Beddoes, J.C. Designing homogenization-solution heat treatments for single crystal superalloys. *Mat. Sci. Eng. A* **2010**, *527*, 5528–5538.
12. Lifshitz, I.M.; Slyozov, V. The kinetics of precipitation from supersaturated solid solutions. *J. Phys. Chem. Solids* **1961**, *19*, 35–50. [[CrossRef](#)]
13. Mathew, M.D.; Parameswaran, P.; Rao, K.B.S. Microstructural changes in alloy 625 during high temperature creep. *Mater. Charact.* **2008**, *59*, 508–513. [[CrossRef](#)]
14. Ding, Q.Q.; Bei, H.B.; Zhao, X.B.; Gao, Y.F.; Zhang, Z. Processing, microstructures and mechanical properties of a Ni-based single crystal superalloy. *Crystals* **2020**, *10*, 572. [[CrossRef](#)]
15. Huang, M.; Cheng, Z.; Xiong, J.; Li, J.; Hu, J.; Liu, Z.; Zhu, J. Coupling between Re segregation and γ/γ' interfacial dislocations during high-temperature, low-stress creep of a nickel-based single-crystal superalloy. *Acta Mater.* **2014**, *76*, 294–305. [[CrossRef](#)]

16. Long, H.B.; Liu, Y.N.; Mao, S.C.; Wei, H.; Zhang, J.X.; Ma, S.Y.; Deng, Q.S.; Chen, Y.H.; Zhang, Z.; Han, X.D. Effect of chemical composition on particle morphology of topologically close-packed precipitates in a Ni-based single crystal superalloy. *Scripta Mater.* **2018**, *157*, 100–105. [[CrossRef](#)]
17. Zhang, Z.K.; Yue, Z.F. TCP phases growth and crack initiation and propagation in nickel-based single crystal superalloys containing Re. *J. Alloys Compd.* **2018**, *746*, 84–92. [[CrossRef](#)]
18. Wilson, B.C.; Hickman, J.A.; Fuchs, G.E. The effect of solution heat treatment on a single-crystal Ni-based superalloy. *JOM* **2003**, *55*, 35–40. [[CrossRef](#)]
19. Sowa, R.; Goehler, T.; Dankl, L. Microstructural stability of TMS-238 Ni-base superalloy during long-term exposure at high temperature. *Mater. Sci. Technol.* **2021**, *37*, 935–950. [[CrossRef](#)]
20. Zhao, Y.; He, S.; Li, L. Application of Hot Isostatic Pressing in Nickel-Based Single Crystal Superalloys. *Crystals* **2022**, *12*, 805. [[CrossRef](#)]
21. Lv, P.; Liu, L.; Zhao, G.; Guo, S.; Zhou, Z.; Chen, R.; Zhao, Y.; Zhang, J. Creep properties and relevant deformation mechanisms of two low-cost nickel-based single crystal superalloys at elevated temperatures. *Mat. Sci. Eng. A* **2022**, *851*, 143561. [[CrossRef](#)]
22. Shang, Z.; Wei, X.; Song, D.; Zou, J.; Liang, S.; Liu, G.; Nie, L.; Gong, X. Microstructure and mechanical properties of a new nickel-based single crystal superalloy. *J. Mater. Res. Technol.* **2020**, *9*, 11641–11649. [[CrossRef](#)]
23. Liu, X.; Huang, T.; Zhang, J.; Wang, D.; Zhang, J.; Hu, R.; Zhang, J.; Liu, L. Influence of thermal exposure on microstructure and stress rupture property of a Re-containing Ni-based single crystal superalloy. *Intermetallics* **2021**, *136*, 107237. [[CrossRef](#)]
24. Yang, X.; Cui, X.; Yuan, H. Correlations between microstructure evolution and mechanical behavior of a nickel-based single crystal superalloy with long-term aging effects. *Mater. Charact.* **2020**, *169*, 110652. [[CrossRef](#)]
25. Watanabe, H.; Mukai, T.; Kohzu, M.; Tanabe, S.; Higashi, K. Effect of temperature and grain size on the dominant diffusion process for superplastic flow in an AZ61 magnesium alloy. *Acta Mater.* **1999**, *47*, 3753–3758. [[CrossRef](#)]
26. Titus, M.S.; Suzuki, A.; Pollock, T.M. Creep and directional coarsening in single crystals of new γ - γ' cobalt-base alloys. *Scripta Mater.* **2012**, *66*, 574–577. [[CrossRef](#)]
27. Baldan, A. Review progress in ostwald ripening theories and their applications to nickel-base superalloys Part I: Ostwald ripening theories. *J. Mater. Sci.* **2002**, *37*, 2171–2202. [[CrossRef](#)]
28. Aghaie-Khafri, M.; Hajjavady, M. The effect of thermal exposure on the properties of a Ni-base superalloy. *Mat. Sci. Eng. A* **2008**, *487*, 388–393. [[CrossRef](#)]
29. Zhang, Y.J.; Zhang, J.X.; Li, P.; Jin, H.X.; Zhang, W.Y.; Wang, Z.H.; Mao, S.C. Characterization of topologically close-packed phases and precipitation behavior of P phase in a Ni-based single crystal superalloy. *Intermetallics* **2020**, *125*, 106887. [[CrossRef](#)]
30. Kurzydłowski, K.J.; Zielinski, W. $\text{Mo}_2\text{C} \rightarrow \text{M}_6\text{C}$ carbide transformation in low alloy Cr-Mo ferritic steels. *Metal. Sci.* **1984**, *18*, 223–224. [[CrossRef](#)]

Disclaimer/Publisher's Note: The statements, opinions and data contained in all publications are solely those of the individual author(s) and contributor(s) and not of MDPI and/or the editor(s). MDPI and/or the editor(s) disclaim responsibility for any injury to people or property resulting from any ideas, methods, instructions or products referred to in the content.